Electrothermal and Electrochemical Modeling of Lithium-ion Batteries: 3D Simulation with Experimental Validation

ECS Transactions, 61 (27) 105-124 (2014)
10.1149/06127.0105ecst ©The Electrochemical Society

Electrothermal and Electrochemical Modeling of Lithium-ion Batteries: 3D Simulation with Experimental Validation

Clemens Fink[a] and Bernhard Kaltenegger[a]

[a] AVL List GmbH, Graz, Austria

This work presents two lithium-ion battery models which are implemented in the multiphysics software package FIRE®, developed by AVL List GmbH: an efficient electrothermal model based on an empirical voltage/current relationship and a physically based, non-isothermal electrochemical model. The models are applied to a 3D simulation of a high energy lithium-ion pouch battery. Both models are adjusted to measured discharge curves for various currents and temperatures. Then their results are compared and a deep insight into the electrodes is given by the electrochemical model. Here, the importance of 3D effects and temperature influence are pointed out – both effects which are often neglected in electrochemical models presented in literature. Finally, both models are compared to voltage and temperature measurements using a realistic, strongly dynamic driving profile. A highly accurate prediction of the experimental data can be achieved with both models.

Introduction

Mathematical modeling is an essential tool for the design, construction, and operation of battery cells and systems. There are a large number of battery models with various complexities and areas of application. This work focuses on electrothermal (ET) and electrochemical (EC) models for lithium-ion (Li-ion) batteries, in which the length scale of consideration is in the range of ~μm to ~cm. The battery models are implemented in the multiphysics software package FIRE®, developed by AVL List GmbH (9).

ET Model. Several approaches which investigate the transient thermal behavior of Li-ion batteries in detail, by covering the effects of state of charge, electric current and temperature, can be found in literature. Most of these approaches follow the models by Shepherd (10), Unnewehr and Nasar (11), and Nernst, combined with a rejected heat model based on voltage drop due to electric load. The advantage of these models is that they require a small amount of data to calibrate the model to different cell types. Often, these parameters can even be derived from product data sheets. The drawback is the limitation to constant current discharging and charging working modes, which means the relaxation behavior of current pulses to reach steady state of the cell terminal voltage cannot be depicted. This has a significant effect when investigating highly dynamic loading conditions such as standardized or arbitrary drive cycle load profiles. The ET model presented in this work is based on the literature sources mentioned above and has been rearranged to better describe the state of charge, current and temperature dependencies. In addition, the focus is on depicting the dynamic relaxation and time

dependent behavior of the battery due to current pulses. The dynamic behavior is described by an additional term consisting of low-pass filtering of the input current signal. This proves to be the most feasible and accurate approach for detailed engineering purposes.

EC Model. Numerous efforts of developing, validating, and applying EC battery models have been reported in the past twenty years. Doyle et al. (7) developed an EC model based on porous electrode and concentrated solution theories which has been adopted and developed further by many authors. Doyle and Newman (1) applied their own EC model to Li-ion polymer batteries and investigated the influence of various adjustable material parameters on the battery performance. Gu and Wang (4) developed a multi-dimensional non-isothermal EC model based on the model by Doyle et al. (7) and pointed out the importance of temperature gradients inside the battery cell. Sikha et al. (3) applied EC models to a Li-ion battery/electrochemical capacitor hybrid system. Smith and Wang (2) used an EC model in order to investigate the behaviour of Li-ion batteries for discharge rates of up to 40 C. Recently, Du et al. (8) developed a surrogate-based multi-scale EC model in which they coupled a 3D microstructure model to a macroscopic homogeneous model. However, most of the EC models presented in literature are used only in one dimension, i.e. normal to the separator, and often temperature effects are not accounted for. The EC model presented in this work is a fully three-dimensional and non-isothermal version of the model by Doyle and Newman (1). It calculates the temporal evolution and spatial distribution of electronic and ionic potentials, Li concentrations in solid particles and electrolyte as well as the temperature for arbitrary load profiles.

The next section covers the theoretical background for both the ET and EC model. The subsequent section describes the simulation setup (geometry, boundary and initial conditions, material and fitting parameters) and the model fitting procedure. Next, simulation results are presented and compared to experimental data and, finally, the work is concluded.

Mathematical Model Description

The first two subsections of this section describe the conservation and transport equations solved in the current collectors and the reaction zone. The third subsection contains the interface coupling conditions and the fourth subsection describes the outer boundary conditions of the modeling domain. Figure 1 shows the assumed battery layer structure in both models.

Current Collectors

In both models, the electronic potential ϕ_{ele} is calculated from the electronic charge conservation equation

$$\nabla \cdot \vec{i}_{ele} = 0 \qquad [1]$$

with the electronic current density $\vec{i}_{ele} = -\sigma_c \nabla \phi_{ele}$. The temperature T is calculated from the energy balance

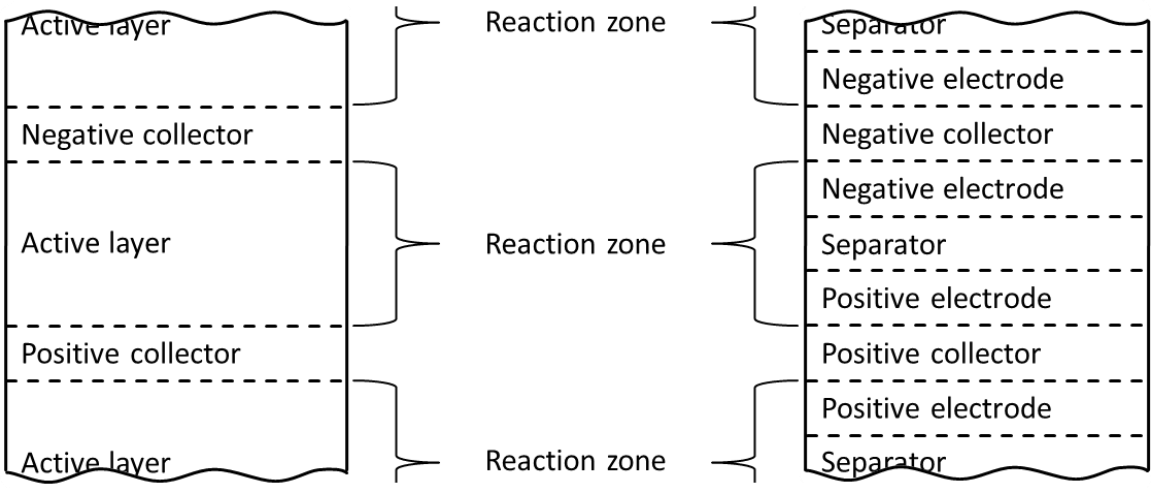

Figure 1. Assumed repeating layer structure in ET model (left) and EC model (right).

$$\frac{\partial\left(\rho_c c_{p,c} T\right)}{\partial t} + \nabla \cdot \vec{\dot{q}} = -\vec{i}_{ele} \cdot \nabla \phi_{ele} \qquad [2]$$

with the conductive heat flux $\vec{\dot{q}} = -\lambda_c \nabla T$.

Reaction Zone

The reaction zone consists of positive electrode, negative electrode, and separator – see Figure 1. In the ET model, both electrodes and separator are combined to an *active layer* in which the reaction heat source is set. Here, the reaction current density, which is calculated from an empirical relation, is prescribed at the interface active layer / current collector – see subsection *Interface Coupling Conditions*. In the EC model, electrodes and separator are spatially resolved and the electrochemical reaction is calculated in the electrode volume at the interface electrode particle / electrolyte.

ET Model. In the active layer the following energy balance is solved:

$$\frac{\partial\left(\rho_{al} c_{p,al} T\right)}{\partial t} + \nabla \cdot \vec{\dot{q}} = \frac{i_{emp}\left(V_{oc,emp} - \Delta\phi_{ele}\right)}{L_{al}} \qquad [3]$$

with the conductive heat flux

$$\vec{\dot{q}} = -\begin{pmatrix} \lambda_{al,x} & 0 & 0 \\ 0 & \lambda_{al,y} & 0 \\ 0 & 0 & \lambda_{al,z} \end{pmatrix} \nabla T \, . \qquad [4]$$

i_{emp} and $V_{oc,emp}$ in equation [3] are reaction current density calculated with equation [20] and local open circuit voltage (OCV) calculated with equation [21] with $K_{I,T} = 1$,

respectively. $\Delta\phi_{ele}$ is the local electronic potential difference between positive and negative electrode and L_{al} is the thickness of the active layer.

EC Model. Electronic potential in the electrodes and ionic potential in the electrolyte are solved from the respective charge conservation equations, i.e.

$$\nabla \cdot \vec{i}_{ele} = -i_r a_s \,,\ \nabla \cdot \vec{i}_{ion} = i_r a_s \qquad [5]$$

with the electronic and ionic current densities

$$\vec{i}_{ele} = -\sigma_s \varepsilon_s \nabla \phi_{ele} \,,\ \vec{i}_{ion} = -\kappa \varepsilon_e^q \left(\nabla \phi_{ion} - \frac{2RT(1-t^+)\nabla c_e}{F c_e} \right), \qquad [6]$$

where the ionic conductivity depends on the Li salt concentration and the temperature, i.e.

$$\kappa = \kappa_{ref}(c_e) \exp\left[\frac{E_{act,\kappa}}{R} \left(\frac{1}{T_{ref}} - \frac{1}{T} \right) \right]. \qquad [7]$$

The reaction current density i_r in the charge conservation equations [5] is calculated with the Butler-Volmer equation according to

$$i_r = i_0 \left[\exp\left(\frac{k_a F}{RT} \eta_{act} \right) - \exp\left(-\frac{k_c F}{RT} \eta_{act} \right) \right] \qquad [8]$$

with the activation overpotential $\eta_{act} = \phi_{ele} - \phi_{ion} - \phi_{oc}$ and the exchange current density

$$i_0 = i_{0,ini} \left(\frac{c_e}{c_{e,ini}} \right)^{k_a} \left(\frac{c_{s,max} - c_{se}}{c_{s,max} - c_{s,ini}} \right)^{k_a} \left(\frac{c_{se}}{c_{s,ini}} \right)^{k_c} \exp\left[\frac{E_{act,i_0}}{R} \left(\frac{1}{T_{ref}} - \frac{1}{T} \right) \right]. \qquad [9]$$

The open circuit potential ϕ_{oc} strongly depends on the surface stoichiometry θ_{se}, i.e. $\phi_{oc} = f(\theta_{se})$ with $\theta_{se} = c_{se} / c_{s,max}$. Under the assumption of spherical electrode particles with an average radius r_s the particle surface area per volume a_s is defined as follows:

$$a_s = \frac{3\varepsilon_s}{r_s} = \frac{3(1-\varepsilon_e-\varepsilon_f)}{r_s}. \qquad [10]$$

The Li concentration in the solid particles c_s and the Li salt concentration in the electrolyte c_e are calculated from the following transport equations:

$$\frac{\partial c_s}{\partial t} - \frac{\partial}{\partial r}\left(D_s \frac{\partial c_s}{\partial r} \right) - \frac{2}{r} D_s \frac{\partial c_s}{\partial r} = 0 \,, \qquad [11]$$

$$\frac{\partial(\varepsilon_e c_e)}{\partial t} + \nabla \cdot \vec{j}_e = \frac{(1-t^+) i_r a_s}{F} \quad [12]$$

with the Li salt diffusion flux $\vec{j}_e = -D_e \varepsilon_e^q \nabla c_e$. The Li diffusion coefficients depend on the temperature, i.e.

$$D_s = D_{s,ref} \exp\left[\frac{E_{act,D_s}}{R}\left(\frac{1}{T_{ref}} - \frac{1}{T}\right)\right], \quad [13]$$

$$D_e = D_{e,ref} + \delta_1 (T - T_{ref}) + \delta_2 (T - T_{ref})^2 + \delta_3 (T - T_{ref})^3 . \quad [14]$$

The state of charge SoC in the EC model is defined as follows:

$$SoC = \frac{\theta - \theta_0}{\theta_1 - \theta_0} \quad [15]$$

with the average stoichiometry $\theta = \bar{c}_s / c_{s,max}$, where the average Li concentration in the particle $\bar{c}_s$ is calculated according to

$$\bar{c}_s = \frac{1}{r_s} \int_0^{r_s} c_s(r,t)\, dr . \quad [16]$$

The maximum battery capacities for each electrode are calculated from geometrical and electrochemical parameters according to

$$Q_{max,+} = \varepsilon_{s,+} V_+ c_{s,max,+} \left(\theta_{0,+} - \theta_{1,+}\right) F \ , \ Q_{max,-} = \varepsilon_{s,-} V_- c_{s,max,-} \left(\theta_{1,-} - \theta_{0,-}\right) F . \quad [17]$$

The electrode particles and the electrolyte are assumed to be in thermal equilibrium, i.e. they share the same temperature field (homogeneous energy approach). The related energy equation reads

$$\frac{\partial\left(\overline{\rho c}_p T\right)}{\partial t} + \nabla \cdot \bar{\vec{q}} = -\vec{i}_{ele} \cdot \nabla \phi_{ele} - \vec{i}_{ion} \cdot \nabla \phi_{ion} + i_r a_s \eta_{act} \quad [18]$$

with the phase averaged conductive heat flux $\bar{\vec{q}} = -\bar{\lambda} \nabla T$.

Interface Coupling Conditions

At the interfaces between battery domains and phases, physical coupling conditions have to be defined in order to catch the non-differentiable (and in some cases discontinuous) nature of solution quantities at these interfaces in a correct way.

ET Model. In the ET model there is only one domain interface: between current collector and active layer. The electronic interface current densities at the side of the collectors $\vec{i}_{c+}^{\,f}$ and $\vec{i}_{c-}^{\,f}$ are calculated as follows:

$$\vec{i}_{c+}^{\,f} \cdot \vec{n}^{\,f} = i_{emp},\ \vec{i}_{c-}^{\,f} \cdot \vec{n}^{\,f} = -i_{emp}, \qquad [19]$$

where the interface normal vector $\vec{n}^{\,f}$ points towards the collector. i_{emp} is a reaction current density calculated iteratively from an empirical equation of the form

$$\Delta\phi_{ele} = V_{oc,emp}^{*} - \eta_{I,T} - \eta_{dyn}, \qquad [20]$$

where

$$V_{oc,emp}^{*} = K_0 + \frac{K_1}{K_5 - DoD\,K_{I,T}} + K_2 DoD + K_3 \ln\left(K_5 - DoD\right) + K_4 \ln\left(DoD + K_5 - 1\right) \qquad [21]$$

is the OCV including the effect of reduced usable capacity for different currents and temperatures via the term $K_{I,T} = f\left(A_I, C_3, C_4, I_{emp}, Q_{max}, \Delta T\right)$. The depth of discharge DoD is defined as

$$DoD = \frac{1}{Q_{max}} \int I_{emp}(t)dt = 1 - SoC \qquad [22]$$

and the temperature difference $\Delta T = T - T_{ref}$. $\eta_{I,T}$ and η_{dyn} in equation [20] are voltage losses attributed to current and temperature influence as well as battery dynamics, respectively. These terms depend on a number of fitting parameters, i.e.

$$\eta_{I,T} = f(F_c, R_I, A_I, C_1, C_2, I_{emp}, Q_{max}, \Delta T), \qquad [23]$$

$$\eta_{dyn} = f(n_F, RC_1, \ldots, RC_{n_F}, R_{dyn,1}, \ldots, R_{dyn,n_F}, I_{emp}, Q_{max}, t). \qquad [24]$$

The solution quantity of equation [20] is the empirical reaction current I_{emp} for a given local potential difference $\Delta\phi_{ele}$. By definition, I_{emp} is positive for discharging and negative for charging. i_{emp} is then calculated with the total reaction area of the battery cell A_{emp} according to $i_{emp} = I_{emp} / A_{emp}$. The empirical equation [20] contains the following fitting parameters:

- fitting of OCV: $K_0, K_1, K_2, K_3, K_4, K_5$
- fitting of current effect: F_c, R_I, A_I [25]
- fitting of temperature effect: C_1, C_2, C_3, C_4
- fitting of battery dynamics: $n_F, RC_1, \ldots, RC_{n_F}, R_{dyn,1}, \ldots, R_{dyn,n_F}$

Temperature and conductive heat flux are assumed to be continuous at the interface collector / active layer, i.e.

$$T_c^f = T_{al}^f \,,\; \vec{\dot{q}}_c^{\,f} \cdot \vec{n}^f = \vec{\dot{q}}_{al}^{\,f} \cdot \vec{n}^f \,. \qquad [26]$$

EC Model. In the EC model there are two different domain interfaces: collector / electrode and electrode / separator. In addition, there is a phase interface between the solid electrode particles and the electrolyte. For the electronic and ionic potentials, the coupling conditions

$$\phi_{ele,c}^f = \phi_{ele,\pm}^f \,,\; \vec{i}_{ele,c}^{\,f} \cdot \vec{n}^f = \vec{i}_{ele,\pm}^{\,f} \cdot \vec{n}^f \,,\; \vec{i}_{ion,\pm}^{\,f} \cdot \vec{n}^f = 0 \qquad [27]$$

are applied to the interface collector / electrode and the coupling conditions

$$\vec{i}_{ele,\pm}^{\,f} \cdot \vec{n}^f = 0 \,,\; \phi_{ion,\pm}^f = \phi_{ion,sep}^f \,,\; \vec{i}_{ion,\pm}^{\,f} \cdot \vec{n}^f = \vec{i}_{ion,sep}^{\,f} \cdot \vec{n}^f \qquad [28]$$

are applied to the interface electrode / separator. In the conditions [27] and [28] electric contact resistances are neglected. For the thermal coupling conditions, temperature and conductive heat flux are assumed to be continuous at the interfaces, resulting in

$$T_c^f = T_\pm^f \,,\; \vec{\dot{q}}_c^{\,f} \cdot \vec{n}^f = \vec{\bar{\dot{q}}}_\pm^{\,f} \cdot \vec{n}^f \qquad [29]$$

at the interface collector / electrode and

$$T_\pm^f = T_{sep}^f \,,\; \vec{\bar{\dot{q}}}_\pm^{\,f} \cdot \vec{n}^f = \vec{\bar{\dot{q}}}_{sep}^{\,f} \cdot \vec{n}^f \qquad [30]$$

at the interface electrode / separator. At the phase interface between electrode particle and electrolyte the following coupling condition is used for the calculation of c_s in equation [11]:

$$-\left(D_s \frac{\partial c_s}{\partial r} \right)_{r=r_s} = \frac{i_r}{F} \,. \qquad [31]$$

Finally, interface coupling conditions for the Li salt concentration are defined. They read

$$\vec{j}_{e,\pm}^{\,f} \cdot \vec{n}^f = 0 \qquad [32]$$

at the interface collector / electrode and

$$c_{e,\pm}^f = c_{e,sep}^f \,,\; \vec{j}_{e,\pm}^{\,f} \cdot \vec{n}^f = \vec{j}_{e,sep}^{\,f} \cdot \vec{n}^f \qquad [33]$$

at the interface electrode / separator.

Boundary Conditions

Boundary conditions are defined on the outer boundaries of the modeling domain. At the electric outlet of the positive terminal the boundary current density is calculated from the total battery current according to

$$\vec{i}_{ele,c+}^{\,b} \cdot \vec{n}^{\,b} = -\frac{I^b}{A^b} \qquad [34]$$

where A^b is the total area of the electric outlet. The battery current I^b is defined positive for discharging and negative for charging. At the electric outlet of the negative terminal the electronic potential is fixed, i.e. $\phi_{ele}^b = 0$. On all other outer boundaries, the electronic current density is assumed to be zero, i.e. $\vec{i}_{ele}^{\,b} \cdot \vec{n}^{\,b} = 0$. Two types of thermal boundary conditions are applied. For the battery terminals, adiabatic boundary conditions are used, i.e. $\vec{q}^{\,b} \cdot \vec{n}^{\,b} = 0$. On the other boundaries, the following convection boundary condition is applied:

$$\vec{q}^{\,b} \cdot \vec{n}^{\,b} = \beta\left(T_\infty - T^b\right). \qquad [35]$$

In the EC model, additional boundary conditions have to be prescribed for the ionic potential and the Li salt concentration in the electrolyte. Here, zero flux conditions are applied, i.e. $\vec{i}_{ion}^{\,b} \cdot \vec{n}^{\,b} = 0$ and $\vec{j}_e^{\,b} \cdot \vec{n}^{\,b} = 0$.

Simulation Setup and Model Fitting

A high-energy Li-ion polymer battery of the pouch type (*ePLB C020* by *EiG Corporation*) is investigated, in which Li[NiCoMn]O_2 and graphite are used as positive and negative electrode materials, respectively. Layer numbers and dimensions are taken from (5). Due to symmetric properties of the geometry and the boundary conditions with a symmetry plane located parallel to the battery layers in the middle of the cell, only half of the battery is meshed. Thus, rather than all 34 repeat units, only 17 have to be considered. Figure 2 shows the computational meshes used in both models. Due to the high resolution of the layers in the EC model, the related mesh contains 704.245 computational cells, whereas the mesh for the ET model contains only 105.427 cells. In Table I the boundary and initial conditions for both load cases *Constant Current Discharging* and *Realistic Driving Profile* are listed. The C-rate is calculated from the maximum battery capacity $Q_{max} = 21$ Ah. Note, that for the EC model the initial Li concentration in the electrode particles is calculated from the initial state of charge via equation [15]. Table II contains the material parameters of the current collectors. The collector materials are aluminum (positive) and copper (negative). The thermal properties of the reaction zone for both models are listed in Table III – refer to (5)**.** The values of the active layer in the ET model are calculated with averaging methods described in (5). Tables IV and V contain the material parameters of the electrodes and the electrolyte, respectively, as well as the related sources. Some of these parameters are used as fitting parameters for the EC model – see description of the model fitting procedure below.

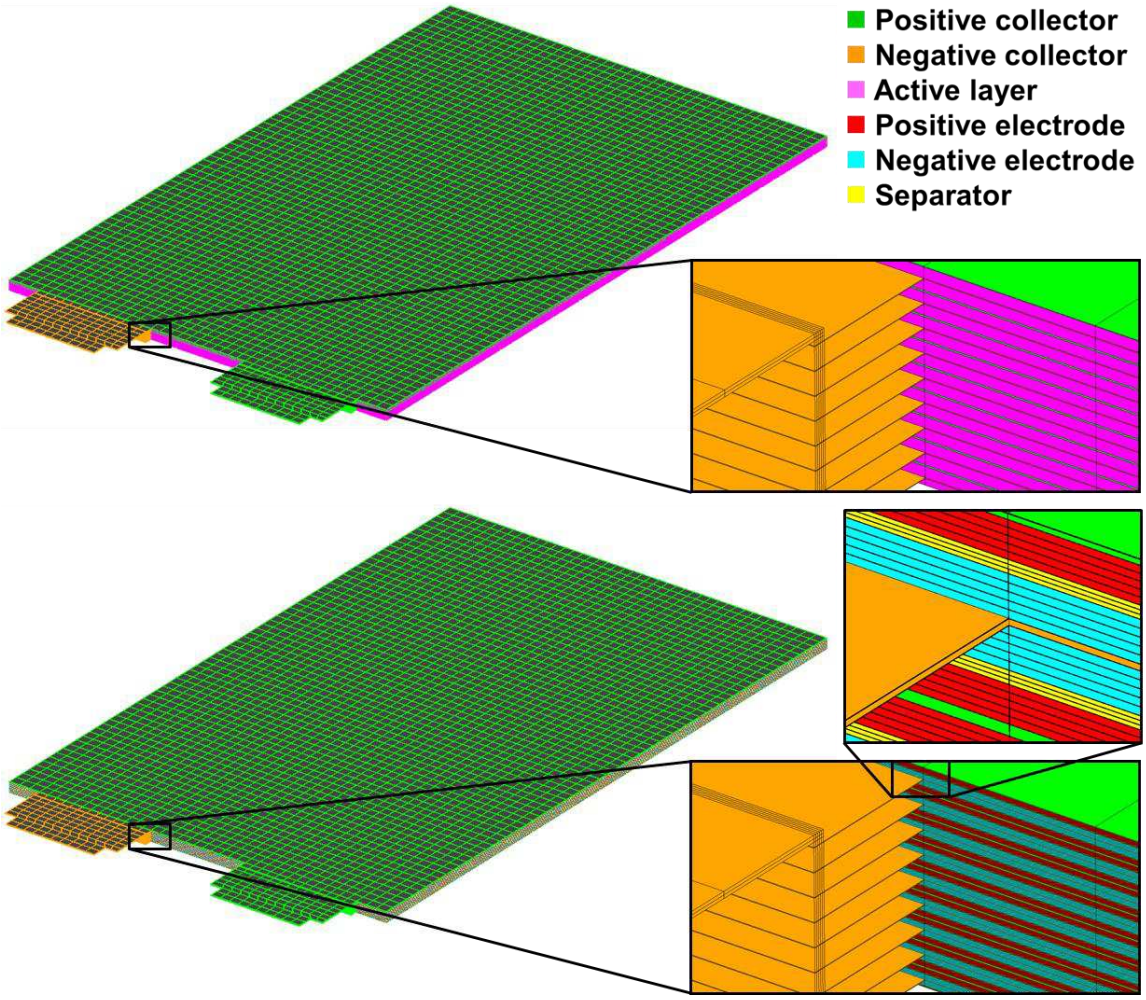

Figure 2. Computational meshes for ET model (top) and EC model (bottom).

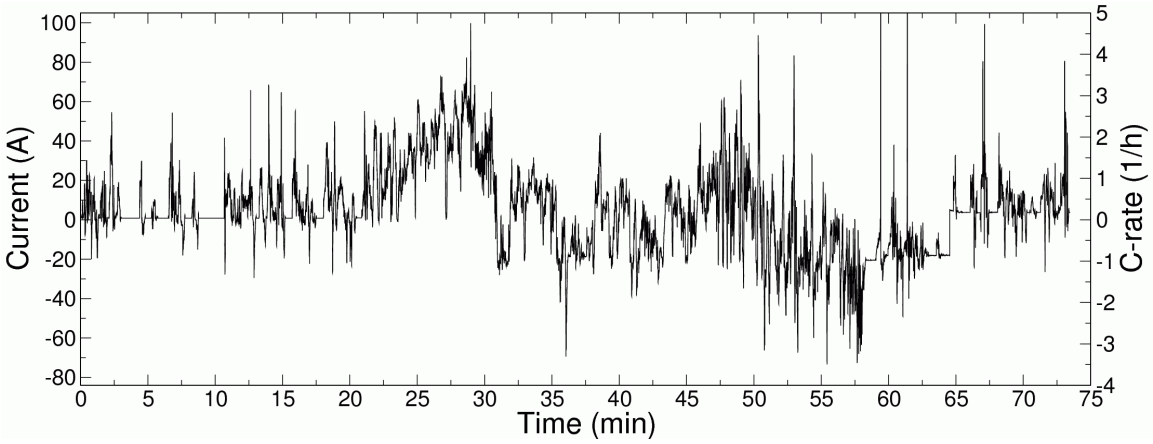

Figure 3. Prescribed current and C-rate of realistic driving profile.

TABLE I. Boundary and Initial Conditions.

Boundary Condition	**Constant Current Discharging**	**Realistic Driving Profile**
Current I^b (A)	4.2, 10.5, 21, 63, 105	$I^b(t)$ – see Figure 3
C-rate (1/h)	0.2, 0.5, 1, 3, 5	$C(t)$ – see Figure 3
Ambient Temperature T_∞ (°C)	-10, 0, 15, 25, 45	25
External Heat Transfer Coefficient β (W/m^{2}K)	25	18
Initial Condition		
State of Charge SoC_{ini} (-)	1	0.924
Temperature T_{ini} (°C)	-10, 0, 15, 25, 45	25
Li Concentration in Electrode Particle $c_{s,+,ini}$ / $c_{s,-,ini}$ (mol/m^3)	5259 / 23191	8581 / 21438
Li Salt Concentration in Electrolyte $c_{e,ini}$ (mol/m^3)	2000	2000

TABLE II. Material Parameters of Current Collectors.

Parameter	**Positive Collector**	**Negative Collector**
σ_c (A/Vm)	3.83×10^7	6.33×10^7
λ_c (W/mK)	238	398
ρ_c (kg/m^3)	2700	8960
$c_{p,c}$ (J/kgK)	900	385

TABLE III. Thermal Properties of Reaction Zone for Both Models (5).

Parameter	**Active Layer (ET Model)**	**Positive Electrode (EC Model)**	**Separator (EC Model)**	**Negative Electrode (EC Model)**
$\lambda_{al,\perp}$ / $\lambda_{al,\parallel}$, $\overline{\lambda}$ (W/mK)	0.898 / 1.157	1.58	0.34	1.04
$\rho_{al}c_{p,al}$, $\overline{\rho c}_p$ (J/m^{3}K)	2.78×10^6	3.68×10^6	2.01×10^6	2.23×10^6

TABLE IV. Material Parameters of Electrodes for EC Model.

Parameter	**Positive Electrode**	**Negative Electrode**	**Source**
ε_e (-)	0.63	0.503	(1)
ε_f (-)	0.073	0.026	(1)
ε_s (-)	0.297	0.471	(1)
r_s (m)	8.5×10^{-6}	12.5×10^{-6}	(1)
σ_s (A/Vm)	2	68.6	(1)
$i_{0,ini}$ (A/m^2)	2	2.75	Fitting
k_c, k_a (-)	0.5	0.5	(1)
ϕ_{oc} (V)	$f(\theta_{se,+})$	$8 + 5.06\,\theta_{se,-} - 12.58\,\theta_{se,-}^{0.5} - 8.63\times10^{-4}\theta_{se,-}^{-1} + 2.18\times10^{-5}\theta_{se,-}^{1.5} - 0.46\exp\left[15\left(0.06-\theta_{se,-}\right)\right] - 0.55\exp\left[-2.43\left(\theta_{se,-}-0.92\right)\right]$	Fitting, (6)
$c_{s,\max}$ (mol/m^3)	51554	30555	(3)
$D_{s,ref}$ (m^2/s)	1.0×10^{-13}	3.9×10^{-14}	(1)
θ_0 (-)	0.95	0.004	Fitting
θ_1 (-)	0.102	0.759	Fitting
T_{ref} (°C)	25	25	(1)
E_{act,i_0} (J/mol)	50000	30000	Fitting, (4)
E_{act,D_s} (J/mol)	20000	4000	(4)

TABLE V. Material Parameters of Electrolyte for EC Model.

Parameter	Value / Function	Source
κ_{ref} (A/Vm)	$1.08\times10^{-2}+6.75\times10^{-4}c_e-5.22\times10^{-7}c_e^2+1.36\times10^{-10}c_e^3-1.17\times10^{-14}c_e^4$	(1)
$D_{e,ref}$ (m^2/s)	7.5×10^{-11}	(1)
q (-)	3.3	(1)
t^+ (-)	0.363	(1)
T_{ref} (°C)	25	(1)
$E_{act,\kappa}$ (J/mol)	5000	Fitting
δ_1 (m^2/Ks)	5.99×10^{-12}	Fitting
δ_2 (m^2/K^2s)	1.76×10^{-13}	Fitting
δ_3 (m^2/K^3s)	1.71×10^{-15}	Fitting

Model Fitting Procedure

Both models are adjusted separately to measured voltage curves with constant discharge currents (0.2, 0.5, 1, 3, 5 C) for an ambient temperature of 25 °C and various ambient temperatures (-10, 0, 15, 25, 45 °C) for a discharge rate of 0.5 C.

ET Model. The fitting parameters in the empirical voltage/current relationship [20] are varied during an automatic fitting procedure in order to match the calculated with the measured voltage curves. Here, the fitting procedure is done in 0D independent of the 3D simulation, i.e. the current I_{emp} is constant for each case and $\Delta\phi_{ele}$ is replaced with the battery voltage. In order to achieve a better fitting result, the temperature increase of the battery is estimated with a 0D thermal model and it is, additionally, included in the fitting procedure. The resulting fitting parameters (see listing [25]) are used in the 3D simulation in order to calculate temperature and potential distribution. The voltage curves obtained with the 3D simulation are shown in Figure 4 and Figure 5.

EC Model. The model fitting of the EC model is more complicated than of the ET model, since it is not straightforward. Often the exact values for many material and reaction parameters are not known, which results in a large number of possible fitting parameters. However, many of them have similar effects on the resulting voltage curves, e.g. both a decrease of the electrode's solid phase electrical conductivity and a decrease of the exchange current density leads to a negative vertical shift of the voltage curve. The authors of this work could identify about ten useful fitting parameters from the large pool of material and reaction parameters. In order to save calculating time, the model fitting is conducted on a reduced computational mesh consisting of one repeat unit, i.e. one pair of collectors, one pair of electrodes, and a separator. The required sub-steps of the fitting procedure and the fitting parameters used for each step are listed below:

1. Fitting of maximum battery capacity $\Rightarrow (\theta_{0,+}-\theta_{1,+})$, $(\theta_{1,-}-\theta_{0,-})$
2. Fitting of open circuit potential vs. SoC $\Rightarrow \phi_{oc,+}=f(\theta_{se,+})$, $\theta_{1,+}$, $\theta_{1,-}$
3. Fitting of voltage vs. capacity for small discharge rates (0.2 C, 0.5 C, 1 C) with insignificant temperature increase $\Rightarrow i_{0,ini,+}$, $i_{0,ini,-}$
4. Fitting of voltage vs. capacity for different temperatures and a small discharge rate (0.5 C) $\Rightarrow E_{act,i_{0,+}}$, $E_{act,\kappa}$, δ_1, δ_2, δ_3

5. Checking of voltage vs. capacity for large discharge rates (3 C, 5 C) with significant temperature increase and refitting, if necessary

ad 1.: It is assumed that both electrodes have the same maximum capacity, i.e. $Q_{max,+} = Q_{max,-} = Q_{max}$ – refer to equation [17].

ad 2.: For the negative electrode $\phi_{oc,-} = f\left(\theta_{se,-}\right)$ is given by (6) (see Table IV), whereas for the positive electrode the dependency of the open circuit potential on the surface stoichiometry is derived from measured OCV curves including $\phi_{oc,-}$.

ad 4.: In order to achieve a more accurate fitting result, for the temperature dependency of D_e a cubic polynomial is used rather than an exponential function – see equation [14].

The obtained fitting parameter values (see tables IV and V) are applied to a 3D simulation on the full computational mesh from Figure 2 bottom. Figure 4 and Figure 5 show the resulting voltage curves.

Results and Discussion

Two load case scenarios are considered:

- *Constant Current Discharging*: various, but constant discharge currents and ambient temperatures
- *Realistic Driving Profile*: strongly dynamic current profile including periods of discharging and charging – see Figure 3

For both load cases, simulation results obtained with AVL FIRE® are compared to experimental data by AVL List GmbH. In the experiments, the battery is surrounded by a box in order to avoid different cooling conditions due to inhomogeneous air flow and enable natural convection from the battery surface inside the box. Beside the voltage response of the battery, the surface temperature is measured with ten thermocouples distributed over the battery surface.

Constant Current Discharging

Figure 4 shows the voltage response to various discharge rates (0.2 C to 5 C) for an ambient temperature of 25 °C and the related evolution of the average temperature, both vs. capacity. The simulation results from both battery models (lines) are compared to the measurements (symbols). For both models, an excellent agreement with the experimental data can be achieved in the entire operating range. Only for the highest C-rate the voltage is slightly overestimated by the simulation. Battery voltage vs. capacity for various ambient temperatures (-10 °C to 45 °C) and a discharge rate of 0.5 C is shown in Figure 5. Again, simulation results obtained with both models are compared to experimental data. Although also here the overall agreement of simulation with measurement is good, a slightly better result can be achieved with the ET model, especially for temperatures below 25 °C. The ET model offers a simple handling of the temperature influence in the model fitting, whereas the fitting in the EC model for various temperatures is difficult due to the complex temperature dependency of the equations and the material parameters.

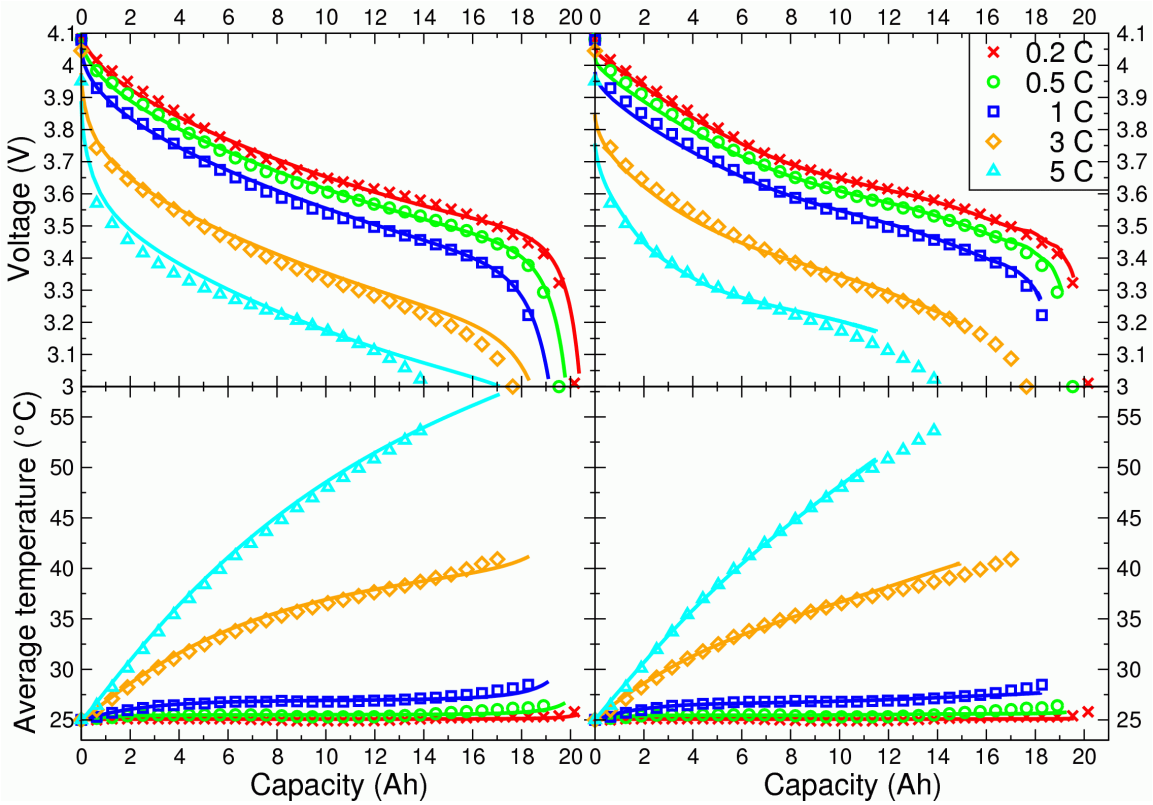

Figure 4. C-rate variation for an ambient temperature of 25 °C: voltage (top) and average temperature (bottom) vs. capacity in experiment (symbols) and simulation (lines) with ET model (left) and EC model (right).

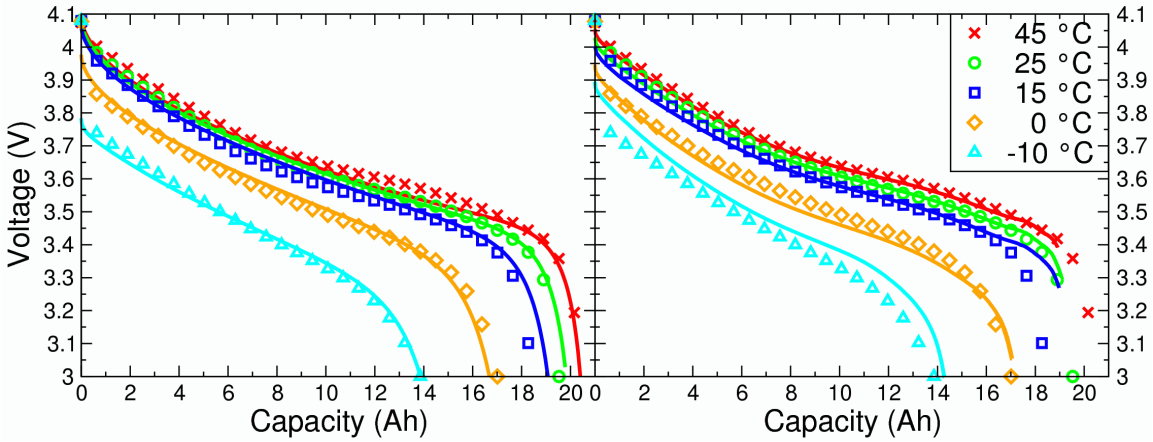

Figure 5. Ambient temperature variation for a discharge rate of 0.5 C: voltage vs. capacity in experiment (symbols) and simulation (lines) with ET model (left) and EC model (right).

Figure 6 shows the surface temperature distribution in both models for discharge rates of 1 C and 5 C and an ambient temperature of 25 °C at a capacity of 11.5 Ah. The results of both models are practically identical. The temperature at the battery boundary is lower than in the center, which is caused by the cooling boundary conditions. However, the largest temperature gradients can be found in lateral rather than in normal direction due to the temperature maxima at the terminals. The latter is caused by the high current density at this location. Whereas for a discharge rate of 1 C the temperature difference across the cell is only 0.4 °C, a discharge rate of 5 C produces a temperature difference of 9 °C. Such relatively large temperature gradients have non-negligible effects on transport properties in the electrodes causing strong lateral non-uniformity of, e.g., Li concentrations, see Figure 8.

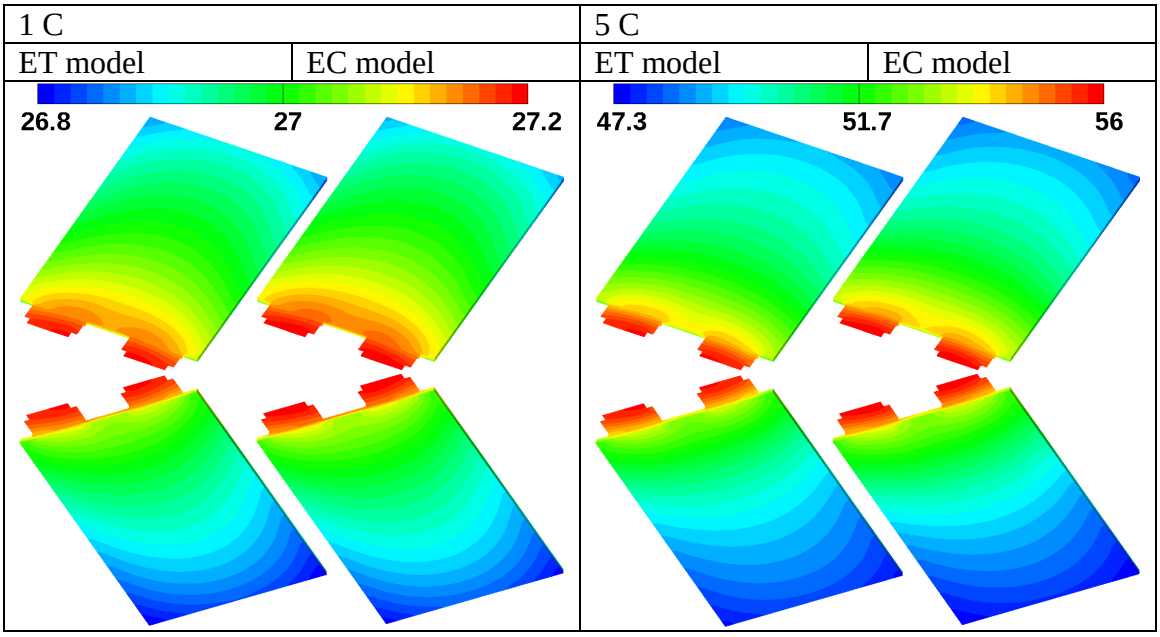

Figure 6. Surface temperature (°C) in both models for a discharge rate of 1 C (left) and 5 C (right) and an ambient temperature of 25 °C at a capacity of 11.5 Ah; top: view of battery center, bottom: view of battery boundary.

Figure 7 shows the SoC distribution in both models for discharge rates of 1 C and 5 C and an ambient temperature of 25 °C at a capacity of 11.5 Ah. Whereas in the ET model the SoC is a 2D quantity for each reaction layer, in the EC model the SoC varies, additionally, in the normal direction of the electrodes. The Soc minimum is located at the terminals due to better electron access and, hence, faster discharging at this location. Although, in the EC model, the largest SoC gradients arise in the normal direction of the electrodes, for a discharge rate of 5 C the maximum lateral SoC difference is, nevertheless, 15 % from the difference in the normal direction.

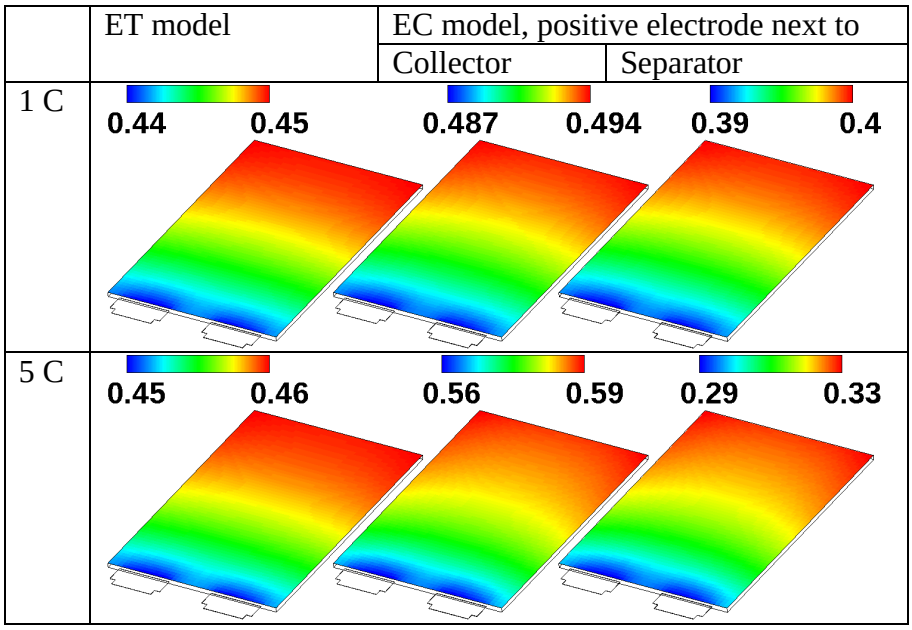

Figure 7. SoC (-) in both models for a discharge rate of 1 C (top) and 5 C (bottom) and an ambient temperature of 25 °C at a capacity of 11.5 Ah displayed in battery center.

Figure 8 shows Li concentration on the particle surface, Li salt concentration in the electrolyte, and volumetric reaction current in the negative electrode. The results obtained with the EC model are shown for discharge rates of 1 C and 5 C and an ambient temperature of 25 °C at a capacity of 11.5 h. The results are displayed in four planes of the negative electrode: in the battery center and at the battery boundary next to collector and separator, respectively. For a discharge rate of 5 C, the large temperature gradients and the low Li diffusion coefficient in the negative electrode particles cause very strong lateral gradients at the interface to the collector: Maximum lateral differences of 82 %, 28 % and 27 % from the differences in the normal direction are obtained for the Li concentration on the particle surface, in the electrolyte, and the reaction current, respectively. For a discharge rate of 1 C the lateral gradients are practically negligible. These results show that the significance of the 3D effect is crucial for large batteries and high discharge rates. The temperature difference between battery center and boundary (see Figure 6) also has a visible effect on the reaction current: In the battery center the reaction current is larger due to the larger exchange current densities at higher temperatures.

Realistic Driving Profile

Figure 9 shows the voltage response to the dynamic current profile from Figure 3 and the average battery temperature in simulation and experiment. Both models are able to predict the voltage response with high accuracy. However, in the periods of charging (see right sub-plot) the voltage is slightly overestimated by the ET model, whereas the EC model approximates the measured voltage more closely. The average temperature is predicted very accurately by both models.

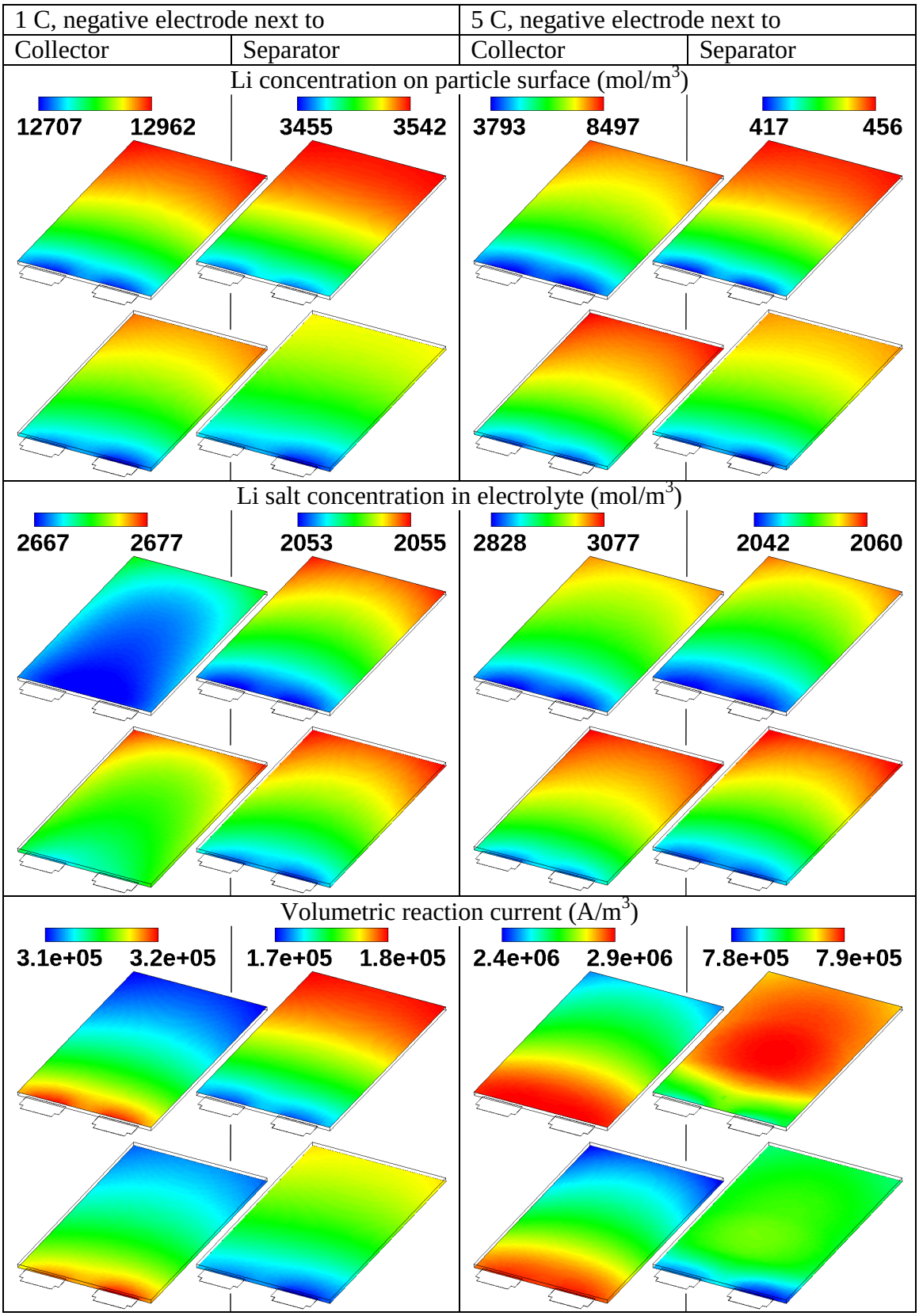

Figure 8. Various quantities from the EC model for a discharge rate of 1 C (left) and 5 C (right) and an ambient temperature of 25 °C at a capacity of 11.5 Ah; displayed in battery center (top) and next to battery boundary (bottom) for each quantity.

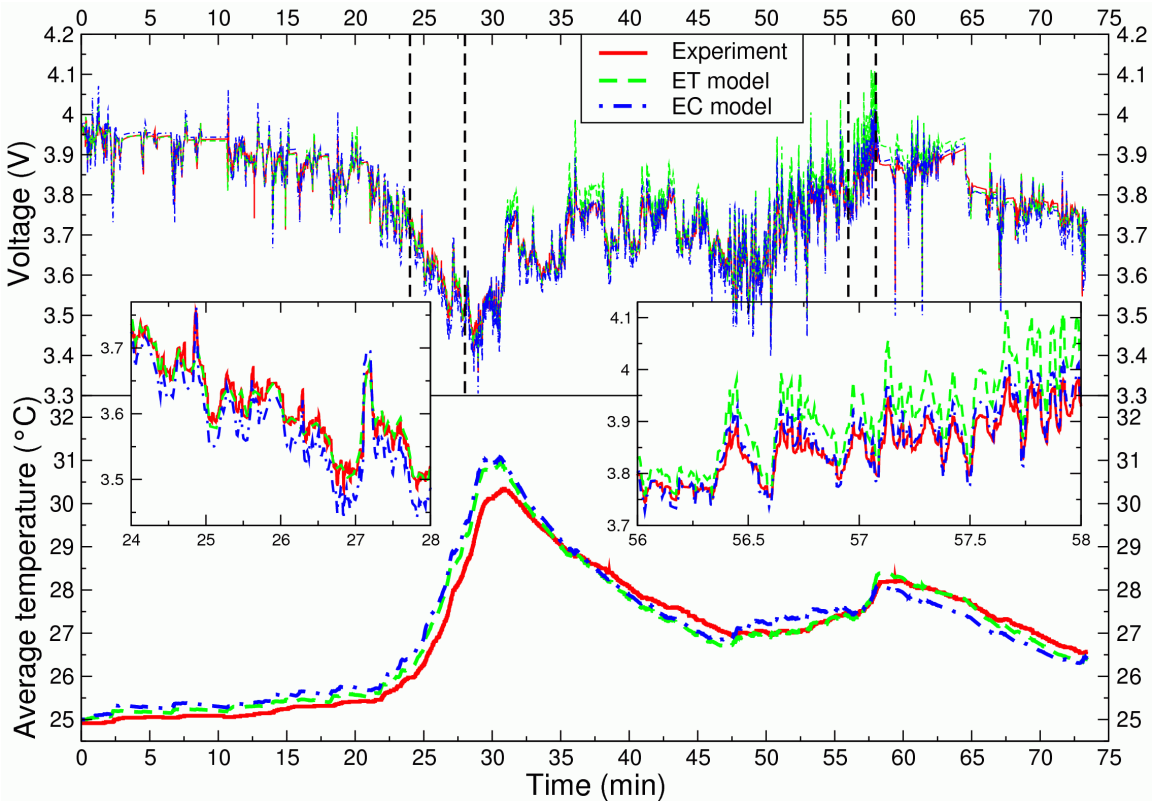

Figure 9. Realistic driving profile: voltage (top) and average temperature (bottom) vs. time in experiment and simulation with both models.

Conclusions

Two lithium-ion battery models of different complexity have been presented: an efficient electrothermal model based on an empirical voltage/current relationship and a physically based, non-isothermal electrochemical model. The models, which are both part of the software AVL FIRE®, have been compared to each other and to experimental data. Each model was able to predict the measured voltage drop and temperature increase during discharging for different operating currents and temperatures. Voltage response and temperature evolution for a realistic driving profile could be predicted by both models with high accuracy as well. It has been demonstrated that – at least for high energy batteries – the inclusion of 3D and temperature effects in the EC model is important for discharge rates larger than 1 C.

Since the simulation with the ET model is a lot faster than with the EC model, the ET model is suitable for the simulation of battery modules and packs. However, the usage of the ET model is limited to the fitted operating range. The EC model is suitable for the simulation of battery cells and delivers a deep insight into the reaction layers, e.g. 3D distribution of lithium concentrations or reaction currents. It also allows for an investigation of material parameters on the performance and should be able to predict the battery behavior of operating conditions beyond the fitted experimental data, e.g. effect of high temperatures during a thermal runaway. Future work includes the application of the ET and the EC model to the simulation of short-circuits in Li-ion batteries and estimation of state of health with the EC model.

List Of Symbols

a_s	active surface area per volume, m^2/m^3
A	area, m^2
A_I	current fitting parameter in ET model, s
c_e	Li salt concentration in electrolyte, mol/m^3
c_p	specific heat capacity, J/kgK
c_s	Li concentration in electrode particle, mol/m^3
C	C-rate, 1/h
C_1	temperature fitting parameter in ET model, $Vs^{0.65}$
C_2	temperature fitting parameter in ET model, 1/K
C_3	temperature fitting parameter in ET model, $s^{0.65}$
C_4	temperature fitting parameter in ET model, 1/K
D	diffusion coefficient, m^2/s
DoD	depth of discharge, –
$E_{act,\varphi}$	activation energy in temperature dependency of φ, J/mol
$f(\varphi)$	function of φ, unit varies
F	Faraday constant, F = 96487 As/mol
F_c	charge factor in ET model, –
i, $\vec{i}$	current density, A/m^2
i_r	reaction current density, A/m^2
i_0	exchange current density, A/m^2
I	electric current, A
$\vec{j}$	diffusion flux, mol/m^2s
k_a	anodic transfer coefficient, –
k_c	cathodic transfer coefficient, –
$K_{I,T}$	term quantifying reduced capacity for different currents and temperatures, –
K_0	OCV fitting parameter in ET model, V
K_1	OCV fitting parameter in ET model, V
K_2	OCV fitting parameter in ET model, V
K_3	OCV fitting parameter in ET model, V
K_4	OCV fitting parameter in ET model, V
K_5	OCV fitting parameter in ET model, –
L	layer thickness, m
$\vec{n}^b$	unit normal vector at outer boundary pointing inside the computational domain, –
$\vec{n}^f$	unit normal vector at domain interface, –
n_F	number of lowpass filters, dynamics fitting parameter in ET model, –
q	Bruggeman exponent, –
$\vec{q}$	conductive heat flux, W/m^2

Q_{max} maximum battery capacity, As
r radial coordinate in electrode particle, m
r_s average particle radius, m
R universal gas constant, R = 8.314 J/molK
RC_i time constant in lowpass filter, dynamics fitting parameter in ET model, s
$R_{dyn,i}$ dynamics resistance factor, dynamics fitting parameter in ET model, Vs
R_I internal ohmic resistance, current fitting parameter in ET model, Vs
SoC state of charge, –
t time, s
t^+ cation transference number, –
T temperature, K
T_∞ ambient temperature, K
V volume, m^3
V_{oc} open circuit voltage, V

Greek Symbols

β external heat transfer coefficient, W/m^2K
δ_1 fitting parameter for temperature dependency of D_e, m^2/Ks
δ_2 fitting parameter for temperature dependency of D_e, m^2/K^2s
δ_3 fitting parameter for temperature dependency of D_e, m^2/K^3s
ε phase volume fraction, –
ε_f volume fraction of conductive filler and binder, –
η_{act} activation overpotential, V
η_{dyn} voltage loss attributed to battery dynamics in ET model, V
$\eta_{I,T}$ voltage loss attributed to current and temperature effect in ET model, V
θ average stoichiometry in electrode, –
θ_{se} surface stoichiometry in electrode, –
θ_0 average stoichiometry in electrode at SoC = 0, –
θ_1 average stoichiometry in electrode at SoC = 1, –
κ ionic conductivity, A/Vm
λ thermal conductivity, W/mK
ρ density, J/kgK
σ electronic conductivity, A/Vm
ϕ electric potential, V
ϕ_{oc} open circuit potential, V

Subscripts

al active layer
c current collector
$c+$ positive current collector
$c-$ negative current collector

e	electrolyte phase
ele	electron conducting phase
emp	in conjunction with empirical equation of ET model
ini	initial value
ion	ion conducting phase
max	maximum value
ref	reference value
s	solid phase of electrode particles
se	interface electrode particle / electrolyte
sep	separator
+	positive electrode
−	negative electrode
±	electrode
⊥	through-plane
‖	in-plane

Superscripts

f	domain interface
b	outer boundary

Abbreviations

EC	electrochemical
ET	electrothermal
Li	lithium
OCV	open circuit voltage

References

1. M. Doyle and J. Newman, *J. Electrochem. Soc.*, **143**, 1890 (1996).
2. K. Smith and C. Y. Wang, *J. Power Sources*, **161**, 628 (2006).
3. G. Sikha, R. E. White, and B. N. Popov, *J. Electrochem. Soc.*, **152**, A1682 (2005).
4. W. B. Gu and C. Y. Wang, in *Lithium Batteries*, S. Surampudi, R. A. Marsh, Z. Ogumi, and J. Prakash, Editors, p. 748, The Electrochemical Society Proceedings Series, Pennington, NJ (2000).
5. P. Taheri and M. Bahrami, *SAE Int. J. Passeng. Cars - Electron. Electr. Syst.*, **5**, 164 (2012).
6. M. Doyle and Y. Fuentes, *J. Electrochem. Soc.*, **150**, A706 (2003).
7. M. Doyle, T. F. Fuller, and J. Newman, *J. Electrochem. Soc.*, **140**, 1526 (1993).
8. W. Du, N. Xue, W. Shyy and J. R. R. A. Martins, *J. Electrochem. Soc.*, **161**, E3086 (2014).
9. FIRE® v2013, *Electrification / Hybridization Manual*, AVL List GmbH (2013).
10. C. M. Shepherd, *J. Electrochem. Soc.*, **112**, 657 (1965).
11. L. E. Unnewehr and S. A. Nasar, *Electric Vehicle Technology*, John Wiley, New York (1982).